

Supercritical Thermodynamics of the Rock/Fluid Geothermal System

Mario-César Suárez Arriaga

Mexican Geothermal Association, Patzimba 438, Morelia, Mich., 58090 México

mcsa50@gmail.com

Keywords: Supercritical geothermal fluid, rock/fluid thermodynamics, experimental thermoporoelasticity.

ABSTRACT

The study of supercritical water is important in geothermal science and in many industrial applications, such as supercritical steam turbines, high pressure devices and supercritical cycles. The temperature gradient between the core and the Earth's surface results from a continuous flow of natural heat, embracing all kind of thermal resources that can be classified in terms of their depth, from shallow depths (10^2 m), to medium depths (10^3 m), and to even deeper depths (10^4 m), where the immense temperatures of molten rocks are reached. The rock and fluids in very deep reservoirs are at supercritical thermodynamic conditions, at more than 374°C and pressures larger than 221 bars, having higher fluid density, larger volumetric enthalpy and more heat available. Any geothermal system reaching enough pressure and temperature at some depth can attain supercritical conditions. These systems could provide at least, twenty times as much power, per unit fluid volume, as the normal geothermal steam used today. This paper provides a computational description of water thermodynamics at supercritical conditions and the power it represents. Supercritical water properties are defined in terms of the Helmholtz potential or free energy, and calculated as functions of density or of pressure, and temperature. The shown supercritical properties are internal energy, enthalpy, entropy, specific isochoric heat, specific isobaric heat, compressibility, bulk modulus, Joule coefficient, speed of sound, thermal expansivity and thermal diffusivity. All of them are presented in graphical form. Another aim of this paper is to introduce some rock poroelastic coefficients measured at temperatures between 25°C and 700°C . The rock parameters were measured experimentally in a rock's laboratory.

1. INTRODUCTION

In a near future, the world could have limited petroleum supply, increasing demand with higher oil cost and increasing pollution with environmental impact. There is an urgent need to gradually replace hydrocarbons with other, diversified, and clean primary sources of energy. Deep geothermal energy is one of the main sources able to gradually replace hydrocarbons and nuclear. The intention of this paper is to provide a basic description of the properties and behavior of geothermal water at supercritical conditions in deep reservoirs. These conditions correspond to an enormous energy source that has never been used on Earth.

2. WATER THERMODYNAMICS AND THE CRITICAL POINT OF WATER

Water in geothermal reservoirs covers a wide thermodynamic range, because the temperature gradient between the core and the surface of the Earth is producing a continuous flow of natural heat, going from shallow depths (10^2 m), to medium depths (10^3 m), and to even deeper depths (10^4 m), reaching the immense temperatures of molten rocks ($T > 1000^\circ\text{C}$). The fluids in deep reservoirs are at supercritical thermodynamic conditions ($T > 374^\circ\text{C}$, $p > 221$ bar), with higher fluid density and more heat available. These systems could provide twenty times as much power, as the normal geothermal fluids used today ($T < 360^\circ\text{C}$, $p < 100$ bar).

2.1 Molecular structure of water

Water ($\text{H}_2\text{O} = {}^1\text{H}_2{}^{16}\text{O}$) is a simple substance, but its properties show a complex behavior. Two hydrogen atoms and one oxygen atom make an angle of approximately 104.5 degrees, giving an extraordinary stability to this molecular structure: each hydrogen atom is in line between the oxygen atom on its own molecule and the oxygen atom of a different molecule. The hydrogen bonds have extra attractive energy, causing many of the unusual properties of water: 1) large heat of vaporization, 2) expansion upon freezing, 3) low thermal conductivity, 4) high specific heat, 5) very low compressibility in liquid phase, 6) very high steam compressibility, 7) water is basic and acid at the same time ($\text{pK}_a/\text{b} = 15.74$), 8) water is a universal solvent, 9) water reaches its maximum density at 4°C , and 1 bar; below 4°C , water density declines (figure 1). Water molecular structure is shown in figure 2.

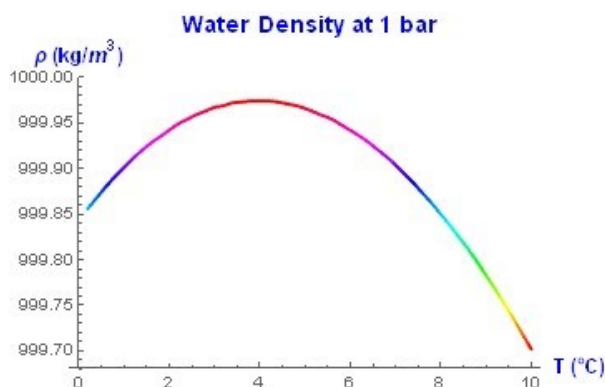


Figure 1: Water density behavior between 0°C and 10°C at the pressure of one bar.

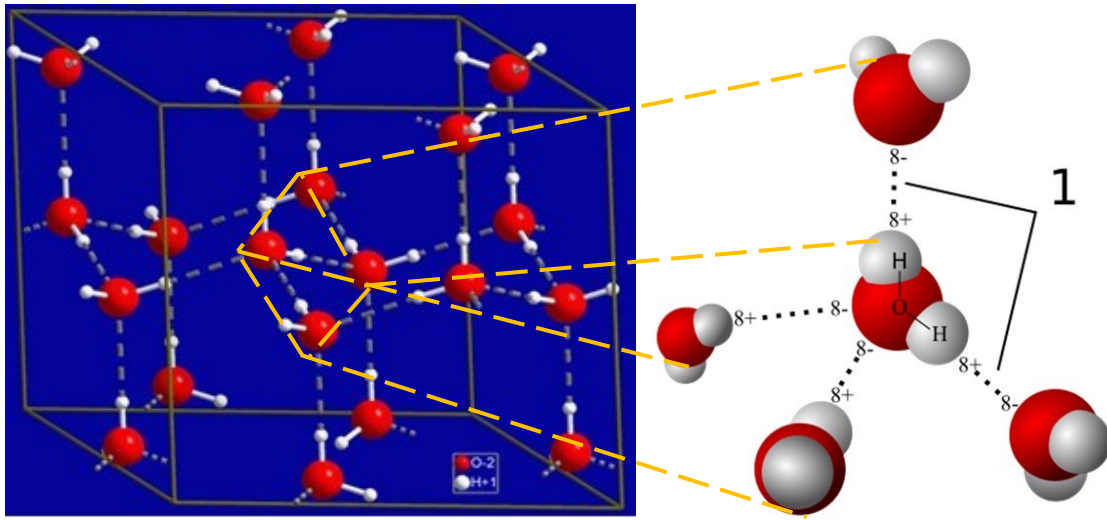


Figure 2: Idealized distribution of water molecules showing its structural bonds. O is in red, H₂ is in light gray. (Illustration adapted from https://en.wikipedia.org/wiki/Hydrogen_bond, Public Domain).

Intermolecular hydrogen bonding is responsible for the high boiling point of water (99.606°C at 1 bar) and its surface tension. The thermodynamic properties of ordinary water are functions of pressure and temperature in single phase systems. In two-phase systems p and T are related in the saturation line (K-Function), and another variable must be used; for example steam quality, liquid saturation or fluid enthalpy. As the critical point is approached the differences between thermodynamic properties of both phases vanish. Once the critical point is reached, the latent heat of vaporization becomes zero and there is no more separation between both phases. In other words, the phase boundary between liquid and vapor disappears. We can also say that the distinction between vapor and liquid ends at the critical point.

2.1.1 Mathematical formulation of water properties

The International Association for the Properties of Water and Steam (IAPWS R6-95, 2016) published in 1995, a worldwide accepted mathematical formulation, which reproduces with maximum accuracy millions of experimental data obtained since 1824 up to present time. Water properties are calculated for single phase, liquid or vapor, as function of density and temperature (ρ, T), and for two-phase water (liquid and steam) pressure p is a function of saturation temperature $p(T_{sat})$. All water properties are constructed in terms of the Helmholtz potential (figure 3) defined as $f_w(\rho, T) = e_w - T s_w$, where e_w is internal energy and s_w is water entropy.

$$f_w(v_w, T) = e_w - T s_w \Rightarrow df_w = -p dv_w - s_w dT \Rightarrow p = -\frac{\partial f_w}{\partial v_w}, s_w = -\frac{\partial f_w}{\partial T} \tag{1}$$

where $v_w = \rho^{-1}$ is specific volume. The potential f_w becomes dimensionless (Φ) as shown in equation (2).

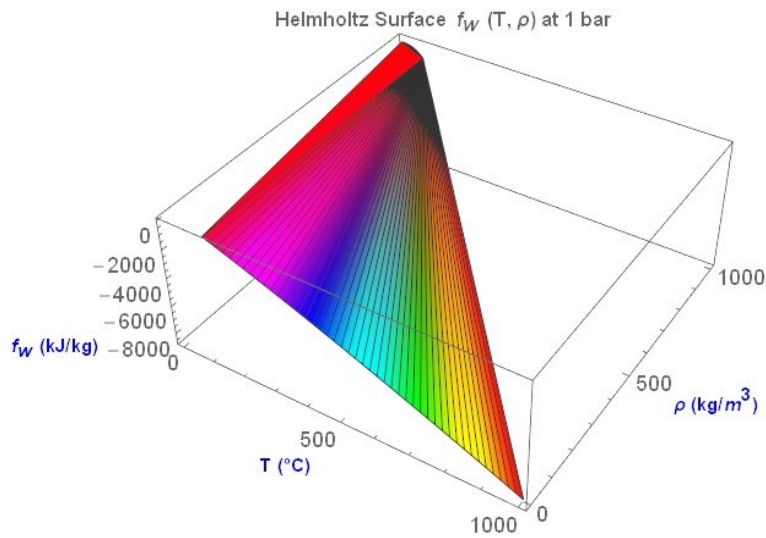


Figure 3: Helmholtz 3D surface for water showing its values at 1 bar of pressure and $0 \leq T \leq 1000$ °C.

$$\delta = \frac{\rho}{\rho_C}, \tau = \frac{T_C}{T} \Rightarrow \frac{f_w(\rho, T)}{R T} = \Phi(\delta, \tau) = \Phi^{gas-ideal} + \Phi^{residual} = \Phi^0(\delta, \tau) + \Phi^r(\delta, \tau) \quad (2)$$

where δ and τ are dimensionless density and inverse temperature respectively; the values of the critical constants are:

$$\rho_C = 322.0 \frac{\text{kg}}{\text{m}^3}, T_C = 647.096 \text{ K}, P_C = 22.064 \times 10^6 \text{ Pa}, \mu_C = 10^{-6} \text{ Pa} \cdot \text{s}, R = 0.46151805 \left[\frac{\text{kJ}}{\text{kg K}} \right]$$

The mathematical form of the ideal gas part (Φ^0) and the residual part (Φ^r) of Φ was built by the *International Association for the Properties of Water and Steam* (<http://www.iapws.org/>):

$$\begin{aligned} \Phi_{gas}^{ideal} = \Phi^0(\delta, \tau) &= \text{Log}(\delta) + n_{01} + n_{02} \tau + n_{03} \text{Log}(\tau) + \sum_{i=4}^8 n_{0i} \text{Log}(1 - e^{-\gamma_{0i} \tau}) \\ \Phi^r(\delta, \tau) &= \sum_{i=1}^7 n_i \delta^{d_i} \tau^{t_i} + \sum_{i=8}^{51} n_i \delta^{d_i} \tau^{t_i} e^{-\delta^{\epsilon_i}} + \sum_{i=52}^{54} n_i \delta^{d_i} \tau^{t_i} e^{-\alpha_i(\delta - \epsilon_i)^2 - \beta_i(\tau - \gamma_i)^2} + \sum_{i=55}^{56} n_i \Delta^{b_i} \delta \psi \end{aligned} \quad (3)$$

Where the auxiliary functions are defined in the Appendix of this paper and all coefficients are in the aforementioned reference.

2.2 Range of validity and definite limits of this formulation for water

The IAPWS R6-95 covers the five phases of water (solid, liquid, steam, two-phase and supercritical), in the entire stable fluid region for $p \in [0.1, 10,000]$ bar, and for $T \in [0, 1000]$ °C (1273 K), reproducing with high precision all the experimental data available at the time the release 2016 of the IAPWS-95 was prepared, including the critical point. The interpolating equations of this formulation can be extrapolated for density and enthalpy beyond the already mentioned limits, giving reasonable accurate results for pressures up to 10^6 bar and temperatures up to 4727 °C (5000 K). All functions and derivatives are computed as functions of (δ, τ). In geothermal fields, for practical reasons, it is more efficient to use the variables (p, T) or (p, h) because water density is not measured. A backward formulation entirely based on the IAPWS-95 was created (Suárez-Arriaga, 2017) using a modified two-dimensional projection of the Newton-Raphson algorithm, which attains convergence in less than four ($n \leq 4$) iterations and [$0 \leq \text{error} \leq 10^{-9}$] (the development of the full algorithm is in the Appendix).

$$\delta_{n+1} = \delta_n - \left(\frac{R \rho_C T_0}{P_C} \left(\delta_n + \delta_n^2 \frac{\partial \Phi^r(\delta_n, \tau_0)}{\partial \delta} \right) - \frac{p_0}{P_C} \right) \frac{\partial \delta}{\partial \Pi}(\delta_n, \tau_0) \Rightarrow \rho(p_0, T_0) \square \dots \quad (4)$$

where: $\left(\frac{\partial \delta}{\partial \Pi} \right)^{-1} = \frac{K_f(\delta, \tau)}{P_C \delta} = \frac{R \rho_C T}{P_C} \left(1 + 2\delta \frac{\partial \Phi^r}{\partial \delta} + \delta^2 \frac{\partial^2 \Phi^r}{\partial \delta^2} \right), \Pi = \frac{p}{P_C}$

where δ_n represents the numerical value of dimensionless density at the n iteration. Figure 4 shows the main regions mentioned in the above paragraph, including the ice zones and the critical point. The supercritical zone is above to the right of this point.

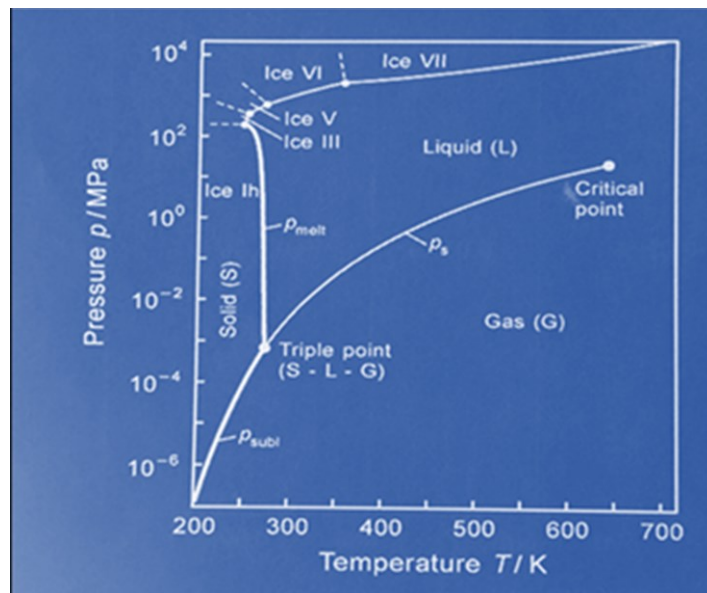


Figure 4: Thermodynamic regions of water projected in a (p, T) plane within the ranges indicated in the figure.

3. WATER THERMODYNAMICS INSIDE THE SUPERCRITICAL REGION

There are several ways to define the 4-dimensional critical point of water. In a pure water temperature-specific volume diagram, the critical point is an inflection point with a zero slope. At this critical point the saturated-liquid and saturated-vapor states become equal in every respect. This “point” is actually a small region located between [373.5, 374.5] °C, showing discontinuities in density between [280, 380] kg/m³ and in enthalpy between [2000, 2150] kJ/kg. In this zone any small change in pressure or in temperature produces wide density and enthalpy changes, allowing many properties of supercritical water to be tuned up. Isobaric specific heat, isothermal compressibility, thermal conductivity, and dynamic viscosity also exhibit large gradients when pressure changes in a neighborhood of the critical point (see figures 7-12). The basic properties of water at the critical point are defined by four specific numerical values: the critical temperature is 374°C ($T_C = 647.096$ K), the critical pressure is 221 bar ($P_C = 22.064$ MPa), the critical density ρ_C is 322 kg/m³, and the critical enthalpy h_C is 2100 kJ/kg (IAPWS R6-95, 2016). At the critical point the densities of the two phases become identical. This collapse of both phases originates discontinuities which are present in all the thermodynamic properties. Above the critical temperature water can exist only as a supercritical fluid and no liquefaction can occur, no matter how high the pressure is raised. One important characteristic of supercritical water is that its solubility capacity increases with pressure in every isothermal curve.

Beyond the critical point (figure 4) there is only one single phase which is called supercritical water defining a whole thermodynamic zone, the supercritical region (figures 5, 6, 7). During any isobaric process at a pressure larger than the critical pressure, or in isothermal processes at temperatures above the critical temperature, there will never be two phases present, because vapor and liquid merge into a single supercritical phase. Only changes in density will be observed when the temperature or the pressure changes. Geothermal fluids are complex mixtures of water, and diverse amounts of salts and gases; obtaining precisely the diverse critical points of these mixtures is a complicated experimental problem not yet solved. But physical intuition indicates that their behavior would be similar or parallel to the behavior of ordinary water in the supercritical region.

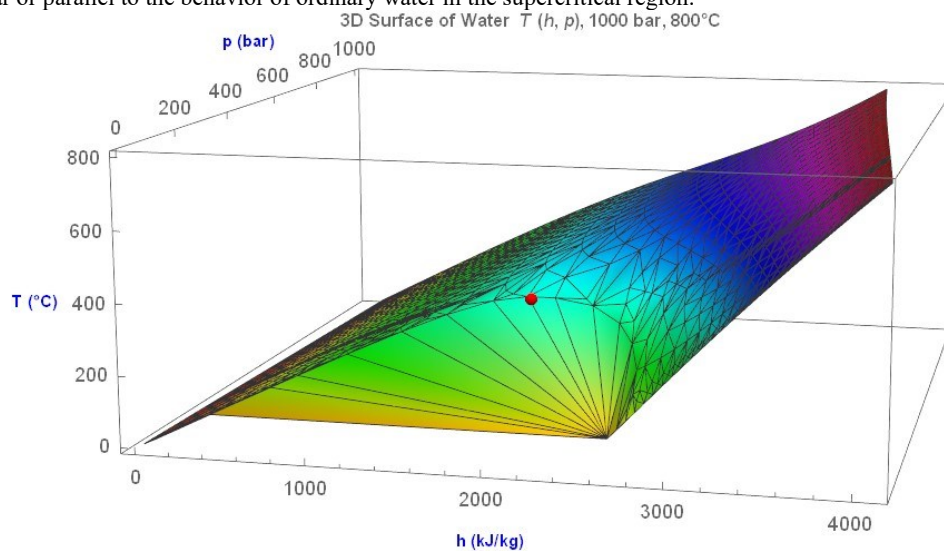


Figure 5. Temperature 3D surface as function of enthalpy and pressure in the range [0, 800] °C.

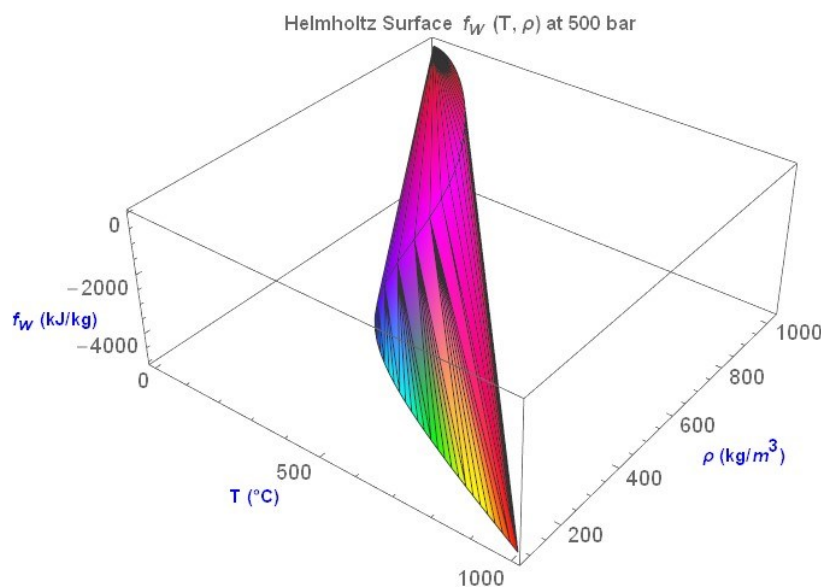


Figure 6. Corresponding 3D Helmholtz surface including the supercritical region of 500 bars

Figures 4 and 5 cover the most common geothermal range for practical use and include a portion of the supercritical zone. The curved region below the critical point in the 3D surface of figure 5, corresponds to the two-phase zone of water. The liquid region is located to the left of this zone, the superheated steam region is above it, and the supercritical zone is up to the right. The red ball shows the approximate location of the critical point in the plane (h , T). Any deep geothermal system reaching enough pressure and temperature can be at supercritical conditions. For example, submarine reservoirs, which are related to the existence of hydrothermal vents emerging in many places along the oceanic spreading centers between tectonic plates. In these sites, hydrothermal fluid at 350°C - 400°C exits the seafloor through natural chimneys at velocities of about 70 to 236 cm/s and mixes with seawater at 4°C at more than 2000 m depth. These systems have a total length of about 65,000 km in the oceanic crust and contain huge amounts of energy. They represent one of the primary modes of interaction between the solid earth and the ocean/atmosphere system (Suárez-Arriaga *et al.*, 2014). The specific chemical characteristics of submarine hydrothermal deep systems indicate that water-oceanic rock interactions occur at supercritical temperature and pressure conditions.

3.1 Main Properties of supercritical water in graphic form

The following figures illustrate the most common thermodynamic properties of water as functions of temperature and pressure in the supercritical region of $[374, 1000]^{\circ}\text{C}$ and $[220, 1000]$ bar. The figures include the region $300^{\circ}\text{C} \leq T \leq 374^{\circ}\text{C}$ as a starting zone. The data were obtained using the NIST/ASME Steam Properties software, version 2.21 (Harvey *et al.*, 2004), which is based on the same formulation (IAPWS-95, 2011).

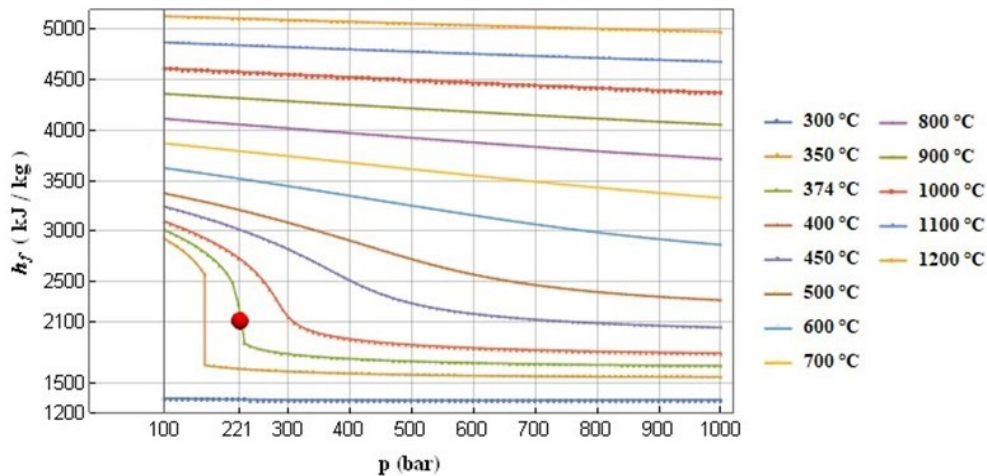


Figure 7. A portion of the supercritical zone projected into the plane (p , h_f) with different temperatures $300 \leq T \leq 1200^{\circ}\text{C}$, the red ball represents the critical point (IAPWS-95 formulation).

3.1.1 Density and enthalpy at supercritical conditions

The following graphics show different water properties as function of temperature for the shown pressures. The values of supercritical density diminished when temperature increases, but they are larger than 120 kg/m^3 at 400°C at the starting pressure of 220 bar (figure 8 left). At higher pressures the supercritical density increases. This physical fact has a huge importance when computing the volumetric enthalpy of supercritical water. The specific water enthalpy increases with temperature and decrease when the supercritical pressure increases (figure 8 right). The missing points in both figures at 220 bars, are real discontinuities near the critical point.

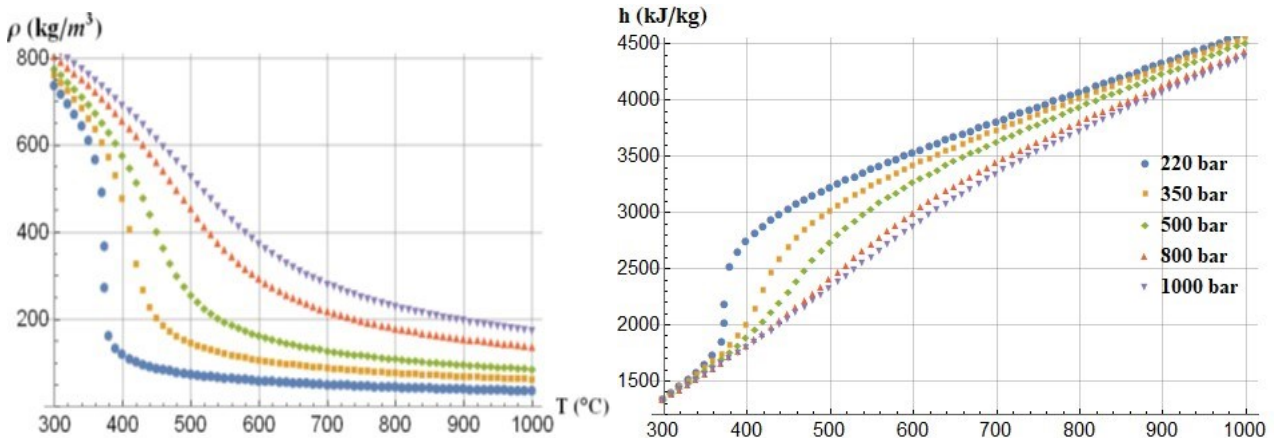


Figure 8. Density (left) and enthalpy (right) in the supercritical zone at different pressures from 220 to 1000 bar.

3.1.2 Dynamic viscosity and thermal conductivity at supercritical conditions

The following figures show that the behavior of both properties is similar in shape: they decrease before the temperatures between 400 and 700°C, at the shown respective pressures (below graphics). After these points, they increase linearly, remaining almost constant. Thermal conductivity clearly shows a region of discontinuity around the critical point.

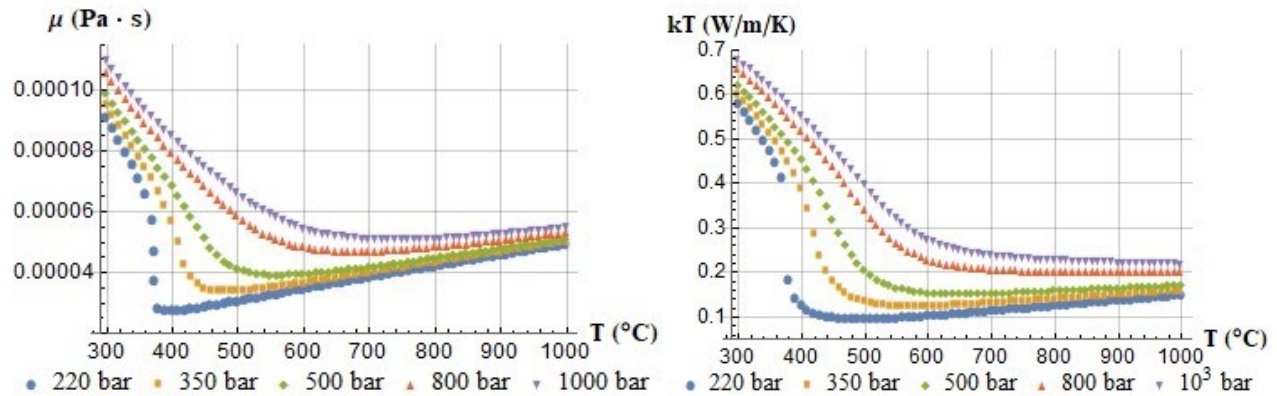


Figure 9. Dynamic viscosity (left) and thermal conductivity (right) in the supercritical zone (pressures are shown below).

3.1.3 Isothermal compressibility and bulk modulus

These two properties are the inverse of each other, but it is interesting to see the behavior of each one of them separately. It is well known that water compressibility increases with temperature before the critical point at any pressure (figure 10 left). In the supercritical zone it decreases after the critical point and remains almost constant when temperature increases (figure 10 left).

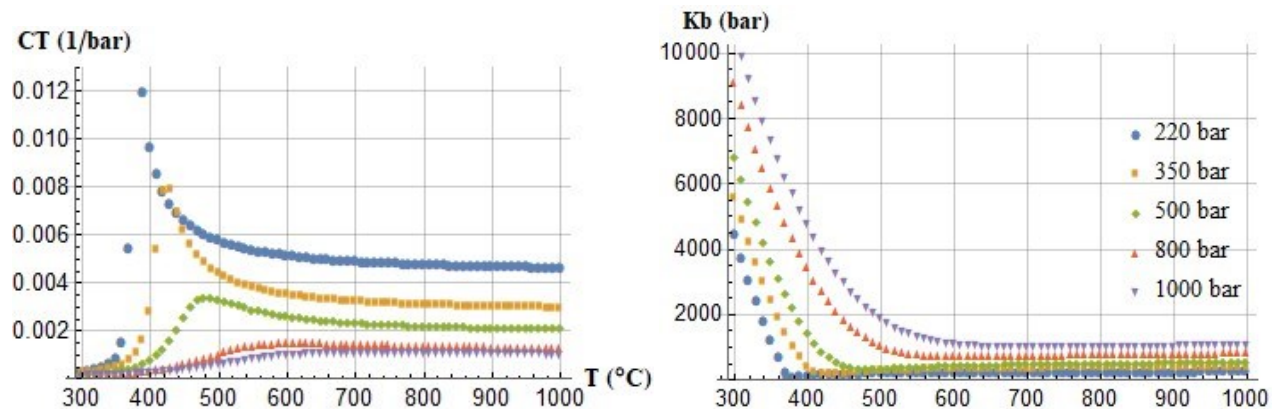


Figure 10. Isothermal compressibility with discontinuities (left) and bulk modulus (right) of supercritical water.

3.1.4 Isobaric specific heat

Figure 11 shows the discontinuous behavior of specific heat c_p , at two different scales which increases beyond any realistic physical limit around 374°C. Extremely high values of c_p have no physical meaning and must be considered as divergent numerical outcomes in the partial differential equations (16f) as explained in (Suárez-Arriaga, 2017).

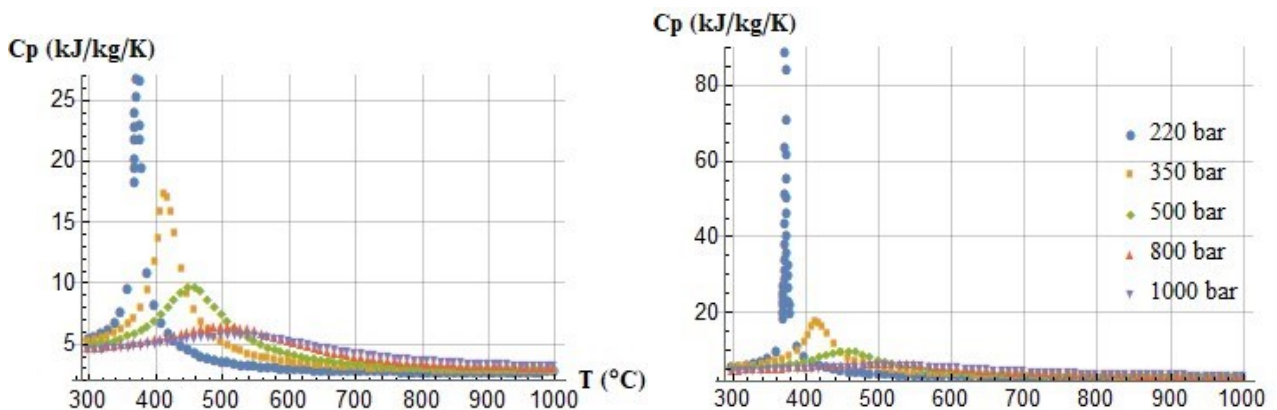


Figure 11. Discontinuity of c_p with sudden increment of specific isobaric heat values around the critical point.

As shown in figure 10, compressibility also shows discontinuities around the critical point. The bulk modulus decreases significantly when temperature rises and increases slightly with supercritical pressures (figure 10 right). It is important to note that its value at 220 bar and 25°C is 2.1 GPa. At 220 bar and 400°C the bulk modulus of water equals 0.0g104 GPa. This means that the bulk modulus in supercritical reservoirs is more than 200 times smaller than in cold aquifers. This coefficient is involved in several relationships among other poroelastic modules (Bundschuh and Suárez-Arriaga, 2010). This numerical difference shows the determinant influence of temperature on rock thermoporoelastic behavior. The main general trend is that rock deformation is larger in geothermal supercritical reservoirs than in normal cold or warm aquifers.

3.1.5 Isobaric specific heat discontinuities in 3D

Figure 12 shows the 3D behavior of isobaric heat c_p in a neighborhood of the critical point (red ball). These graphics were obtained from the IAPWS-95 formulation in dimensionless form (equation 2), equivalently for densities between [241.5, 418.6] kg/m³ and temperatures between [370, 378] °C. These are real numerical singularities, which correspond to the nonlinear equations obtained when fitting the experimental data (equations 16). A similar situation occurs with all other water properties at the critical point.

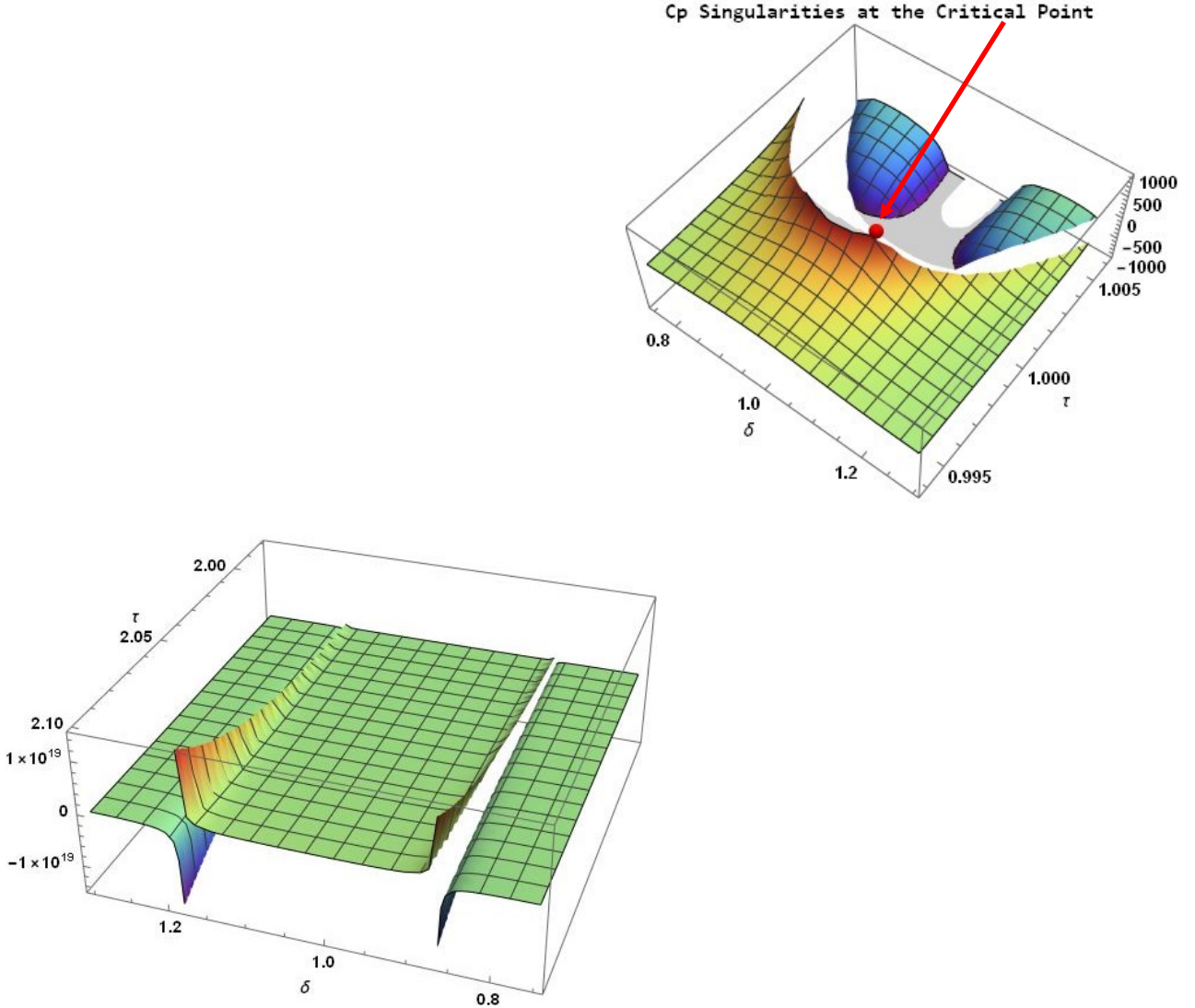


Figure 12. 3D singularities of c_p around the critical point (red ball) in dimensionless form. First graphic (left) shows two branches of discontinuity for $\delta \in [0.75, 1.3]$, $\tau \in [1.98, 2.1]$. Second graphic (right) shows details of the first branch.

3.2 Volumetric enthalpy and exergy of supercritical systems

The change of specific enthalpy in a reservoir is the heat extracted during a process under constant pressure. This change includes both the change of internal energy and the work done; it is equal to the isobaric heat transfer δQ_p during a thermodynamic process:

$$\Delta h_w(p, s_w) = \Delta e_w + p \Delta v_w = (\delta Q_p - p \Delta v_w) + p \Delta v_w = \delta Q_p \quad (5)$$

This is the main reason why the specific enthalpy is the thermodynamic potential commonly used in geothermal reservoir engineering. The product specific enthalpy times water density ($H_w = h_w \rho_w$) is defined as volumetric enthalpy. If the fluid is contained in a porous/fractured rock, the actual fluid enthalpy in the reservoir is affected by porosity ϕ . Therefore, the water enthalpy density of the system at constant pressure or at any isobaric curve is equal to the product:

$$\phi H_w(T) = \phi \rho_w(T) h_w(T) \quad [kJ/m^3] \quad (6)$$

Equation (6) represents the heat stored in the fluid per cubic meter of porous rock as function of supercritical temperature. Figure 13 shows the curves of $\phi H_w(T)$ for different supercritical pressures in a reservoir with 5% porosity. On the other hand, the heat stored in the solid skeleton per unit volume of porous rock is:

$$(1-\phi) H_R(T) = (1-\phi) c_R(T) \rho_R T \quad [kJ/m^3] \quad (7)$$

where ρ_R is rock density and $c_R(T)$ is the isobaric rock specific heat capacity, which is also a function of temperature. A linear, practical correlation to compute $c_R(T)$ is given by this formula (Bundschuh and Suárez-Arriaga, 2010):

$$c_R(T) = 10^{-3} (976.6065 + 0.752854 T) \quad \left[\frac{kJ}{kg \text{ } ^\circ C} \right] \quad (8)$$

Assuming that correlation (8) is valid in a supercritical reservoir, the total volumetric heat stored in the fluid/rock system (figure 13) becomes a quadratic function of temperature.

$$Q_V(T) = \phi H_w(T) + (1-\phi) H_R(T) \quad [kJ/m^3] \quad (9)$$

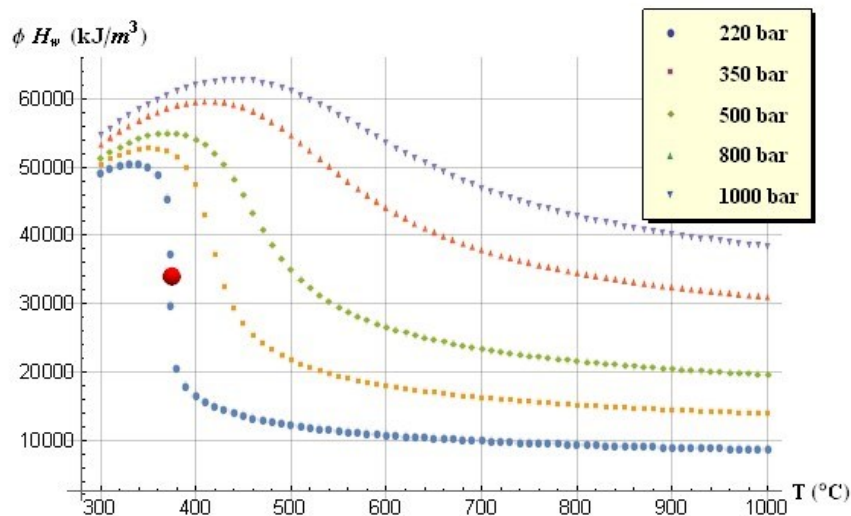


Figure 13. Supercritical volumetric fluid enthalpy in a reservoir with 5% porosity. The red ball is the critical point.

Figure 14 shows the corresponding curves of $Q_V(T)$ for different supercritical pressures. It is observed that Q_V does not depend on pressure because the thermal energy is for the most part stored in the rock. Using the numerical outcomes of figures 12 and 13 we deduce that the fluid enthalpy density represents between 0.08% and 5% of the total stored heat within the reservoir porous rock.

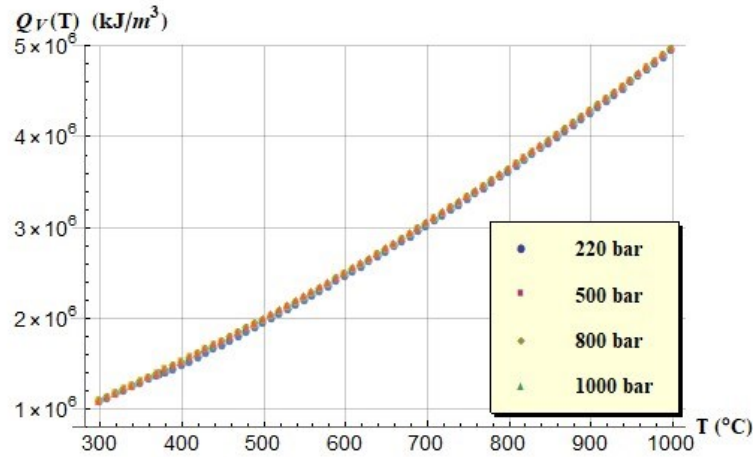


Figure 14. Total volumetric heat in a supercritical fluid/rock system with 5% porosity.

3.3 Exergy of supercritical water

The Exergy is the "maximum work" (power) output that could theoretically be obtained from a system at specified thermodynamic conditions relative to its surroundings. A system may receive (or discharge) fluids from (or to) the surroundings, and exchange heat and work with the surroundings." (DiPippo, 2008). The state of the surroundings is the "dead state" because when a fluid is in equilibrium with the surroundings it may be considered dead, and the exergy from the system is zero. The specific exergy $E_x(T)$ and the maximum power output $dW_{Max}(T)/dt$ from a supercritical reservoir can be computed for a steady, open process as follows (DiPippo, 2008).

$$E_x(T) = h_1 - h_0 - T_0(s_1 - s_0) \left[\frac{\text{kJ}}{\text{kg}} \right] \Rightarrow \frac{dW_{Max}(T)}{dt} = \frac{dm}{dt} E_x(T) \quad [\text{kW}] \quad (10)$$

Where h_1 and s_1 are the specific enthalpy and entropy at the reservoir's outlet, h_0 and s_0 are the specific enthalpy and entropy of the surroundings considered as the dead state, T_0 is the temperature of the dead state and dm/dt is the reservoir mass flow rate. Exergy is also defined as *the maximum available useful work possible during a thermodynamic process that brings the system into equilibrium with a heat reservoir*. A heat reservoir is a system which its heat capacity is so large that when it is in thermal contact with other system its temperature remains constant. In this context, the atmosphere or the deep ocean can be considered as huge heat reservoirs. Both systems can be defined in a stable manner and approximated as unchangeable reference states or dead states. We assume a submarine reservoir discharging directly its supercritical fluid into its surrounding, without considering any losses by friction inside wells or pipes. Figure 15 shows the behavior of the specific exergy from this reservoir as function of temperature, for different supercritical pressures. The thermal values of the dead state correspond to seawater at $T_0 = 4^\circ\text{C}$, $h_0 = 34.4 \text{ kJ/kg}$, $s_0 = 0.046 \text{ kJ/kg/K}$, and a surrounding pressure of 220 bar (Suárez-Arriaga *et al*, 2014).

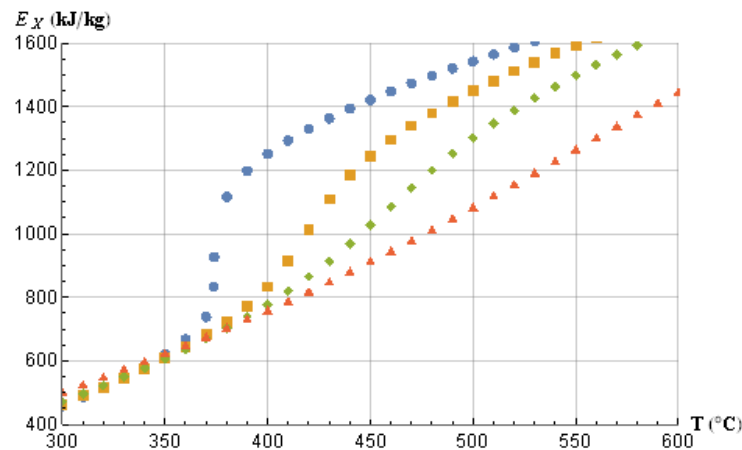


Figure 15. Power output (specific exergy) from a supercritical reservoir.

3.4 Summary of main physical properties of supercritical water

Supercritical water properties are very different from ambient liquid water and from subcritical geothermal water. Inside this region, liquid and steam do not exist, there is only one homogeneous single supercritical phase. Latent vaporization heat is zero, and there is

no surface tension, relative permeabilities disappear. No liquefaction can occur, no matter how much pressure is raised. Supercritical solubility capacity increases with pressure at every isothermal curve. There is experimental evidence of an “*active phase change*”, about CO₂ solubility in a geothermal reservoir. This mechanism leads CO₂ to enter the smallest pore spaces via a chemical gradient, reducing the residual water saturation (Pistone & Horne, 2012). A possible application is the CO₂ sequestration and its use as a working fluid in supercritical EGS. Supercritical fluid is denser (figure 16), has higher enthalpy than common steam at larger pressure and temperature, and has high compressibility, high diffusivity and low viscosity. It is a poor solvent for electrolytes. Under extreme conditions (2.38 g/cm³, 3000 K, 6000 bar), it may be extremely reactive causing explosive reactions. Supercritical water has total miscibility with organic fluids and oxygen in supercritical equilibria.

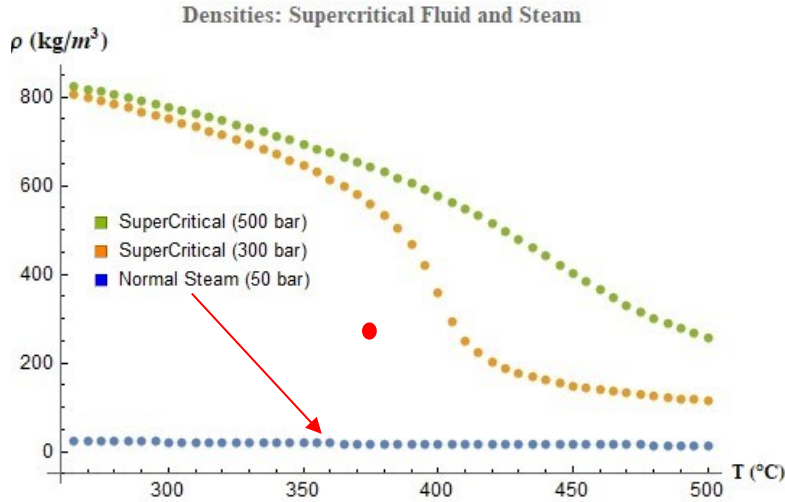


Figure 16. Densities comparison between steam and supercritical water at two pressures. The red ball is the critical point.

Figure 16 illustrates the fact that density of supercritical water is always higher than steam density at any pressure and temperature. This supercritical property is of particular importance because the total mass flow rate Q_m of water flowing to a turbine is directly proportional to fluid density:

$$Q_m = \rho \frac{dV_{fluid}}{dt} \left[\frac{kg}{s} \right] \quad (11)$$

Where ρ is fluid density and V_{fluid} is the variable volumetric flow rate of water.

4. ELECTRICITY GENERATION AND THE SUPERCRITICAL RANKINE CYCLE

The Rankine Cycle is an idealized thermal cycle that converts heat into mechanical work, using hot water as the working fluid inside a turbine. The Carnot thermal efficiency of any Rankine cycle is defined as:

$$\eta_\theta = 1 - \frac{T_{min}}{T_{Max}} \quad (12)$$

where T_{Max} is the temperature of water entering the turbine, and T_{min} is the water outlet temperature after condensation. Supercritical water enhances the efficiency of all traditional steam-power plants. There are two reasons:

- 1) The thermodynamic efficiency of a steam turbine depends on the temperature difference between the vapor and the sink (thermal Carnot cycle, equation 12).
- 2) The higher-pressure operation increases the thermodynamic efficiency of the Rankine cycle.

Therefore, higher fluid temperature means greater potential efficiency. Electric power increases also with higher flow rate, higher temperature and pressure differences. Future supercritical units could increase the Rankine cycle efficiency from 30% up to 53% in turbines operating at supercritical conditions. Supercritical units can increase the cycle efficiency from 35% up to 42% in turbines operating at 250 bar, 600°C. Ultra-Supercritical units at 300 bar and 700 °C will still increase the efficiency up to more than 50 %. For example, steam at $T_{Max} = 140^\circ\text{C}$ enters a turbine; after condensation, $T_{min} = 95^\circ\text{C}$, therefore $\eta_\theta = 32.1\%$. Supercritical fluid enters a turbine at $T_{Max} = 500^\circ\text{C}$, and exits at 235°C ; therefore $\eta_\theta = 53\%$. There is also a huge difference in volumetric enthalpy between steam and supercritical water. Dry steam at 370°C and 40 bar contains 45,354 kJ/m³ of heat. Supercritical fluid at 350 bar and 400°C contains 1 million kJ/m³ of geothermal heat. Supercritical units are the standard for future power plants operating at very high pressures larger than 221 bar.

4.1 Volumetric Enthalpy and the supercritical Rankine Cycle

The Rankine Cycle is an idealized thermodynamic process which describes the way a power plant generates electricity from steam. Figure 17 shows two Rankine cycles for water using a classic diagram (entropy – temperature).

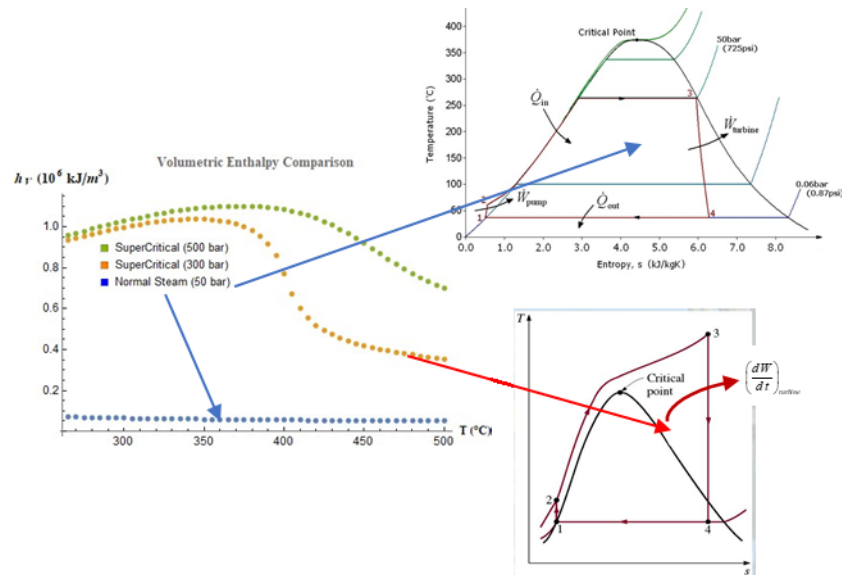


Figure 17. The Rankine cycle for steam and for supercritical water at 300 bar.

Supercritical water improves the Carnot efficiency of a Rankine Cycle converting heat into a larger amount of mechanical work, using the supercritical water as the working fluid, instead of steam, inside a supercritical turbine. The upper right illustration in figure 17 (adapted from https://en.wikipedia.org/wiki/Rankine_cycle#Supercritical_Rankine_cycle, Public Domain) is a normal Rankine steam cycle. The lower right figure represents a supercritical Rankine cycle for an inlet pressure of 300 bar. In both cases, the area inside the closed curve [1-2-3-4] approximates the power (dW/dt) of the water, which performs the mechanical work in the turbine through the fluid expansion during the process [3-4], which produces electricity.

Denser water under supercritical conditions contains much more thermal energy to perform work than geothermal steam, and the corresponding thermodynamic area [1-2-3-4] is larger for increasing supercritical temperatures. This phenomenon occurs because the output power (dW/dt) in the path [3-4] depends on the temperature difference between the supercritical water (heat source) and the outlet colder source or sink because of the Carnot cycle (equation 12). Therefore, the higher the supercritical water temperature, the larger the mechanical work that the fluid will do with much greater efficiency.

5. THERMOPOROELASTIC BEHAVIOR OF VOLCANIC ROCKS

During an academic cooperation agreement with the rock mechanics laboratory of the National Autonomous University of Mexico, (IIM-UNAM), measurements of some poroelastic coefficients were made in volcanic rock cuttings, one from the geothermal field of Los Azufres, Mexico (AZ, andesite with porosity of 5%, courtesy of Comisión Federal de Electricidad), and another one from a core of a geothermal field in Kamchatka, Russia (K1, tuff with porosity of 20%, courtesy of Roman I. Pashkevich, Research Geotechnological Center of the Far Eastern Branch of the Russian Academy of Sciences). The experimental measurements were done with a mechanical test device (Instron 1125). The measurements were made according to the Mexican norm ASTM-C-170 (de la Calleja, E., 2018). The main objective of the project was to measure rock properties in a wide temperature range from 25°C to 700°C, at atmospheric pressure. The poroelastic parameters measured under these conditions were the following:

- 1) F_M , (kN), Vertical Load at Maximum.
- 2) d_M , (mm) Deformation or Vertical Displacement at Maximum.
- 3) σ_M , (MPa), Vertical Stress at Maximum.
- 4) ε_M , (%), Vertical Strain at Maximum corresponding to σ_M .
- 5) F_z (kN) Vertical Load at Yield.
- 6) d_z (mm), Displacement at Yield.
- 7) σ_z (MPa) Stress at Yield.
- 8) ε_z (%) Strain at Yield.
- 9) E_z (MPa) Young Modulus.
- 10) T_e (MPa) Energy of Deformation.
- 11) E_F (J) Energy at the Creep Point.

Figure 18 shows the graphical results of the Young modulus and of the vertical maximum deformation measured in the cutout AZ, while Figure 19 shows the values of the same parameters for the core K1 from Kamchatka.

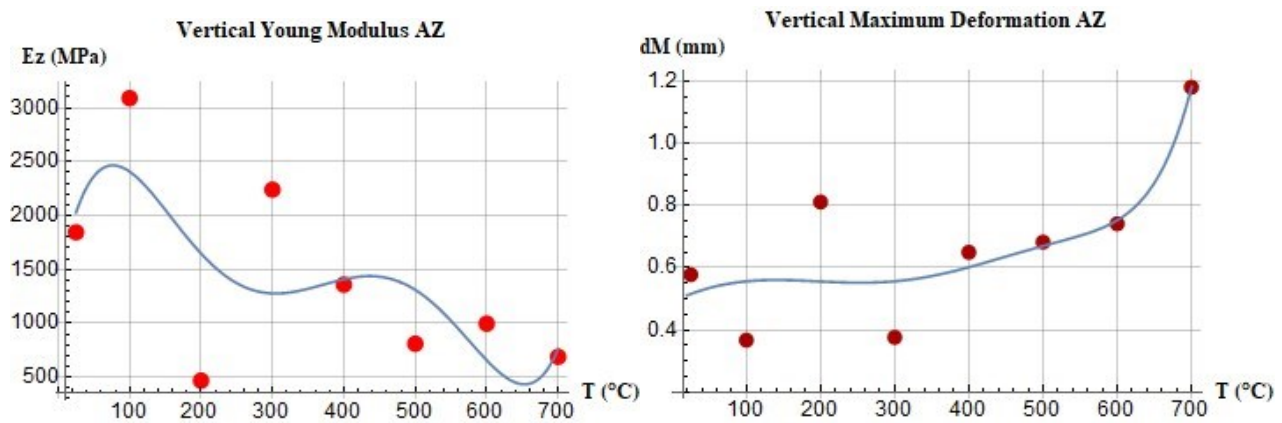


Figure 18. Thermoporoelectric behavior of Young modulus (left) and absolute vertical deformation (right) at 1 bar of pressure and increasing temperatures in a volcanic rock cutout from Los Azufres, Mexico geothermal field.

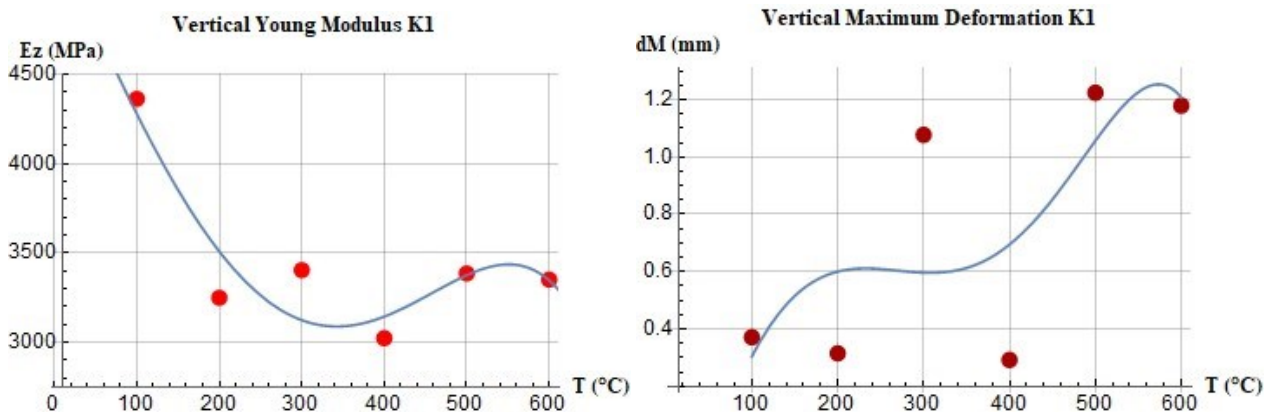


Figure 19. Thermoporoelectric behavior of Young modulus (left) and absolute vertical deformation (right) at 1 bar of pressure and increasing temperatures in a volcanic rock cutout from a Kamchatka, Russia geothermal field.

5.1 Brief discussion of the poroelastic measurements

All measurements exhibit an important random component; this is because the available rock clippings were not homogeneous, presenting important physical heterogeneities, including micro-fissures. However, these experimental results show a clear tendency in Young's modulus to decrease when temperature increases in both types of rock, AZ and K1. This coefficient is a poroelastic parameter defined as the ratio of longitudinal stress to longitudinal strain, in this case, in the vertical direction; it describes the linear response of the porous rock to linear strain $E_z = \sigma_z / \epsilon_z$. Therefore, the obtained results suggest that Young's modulus is a non-linear function of temperature, which diminishes when temperature increases. According to this behavior, the experimental results for strain, show that the vertical maximum deformation of the porous rock increases with increasing temperature, which is quite intuitive, since the hotter rock has less strength. This deformation and the corresponding strain are also non-linear functions of rock temperature.

6. CONCLUSIONS

Water in geothermal reservoirs covers a wide thermodynamic range; H_2O apparently is a simple substance, but its properties show a very complex behavior. Intermolecular hydrogen bonds are responsible of this unusual behavior and of the singularities that appear at a neighborhood of the critical point. Beyond this point, water becomes a supercritical fluid, showing the following properties:

- Deep geothermal heat represents an immense energy potential. The fluids contained in profound reservoirs can be at supercritical thermodynamic conditions. Total supercritical volumetric heat increases with temperature at any pressure.
- Volumetric enthalpy of supercritical water is much larger than in common geothermal fluid because of its higher density. It increases with increasing pressure and decreases slightly with increasing temperature.
- Dry steam at 370°C and 40 bar has a density of 14.43 kg/m³ and contains 45,354 kJ/m³ of heat. The density of supercritical water at 350 bar and 400°C is 475 kg/m³ and contains almost 10⁶ kJ/m³ of geothermal heat.
- Supercritical exergy increases with increasing temperature at any supercritical pressure.
- Supercritical water increases the thermodynamic Carnot efficiency in the Rankine cycle, converting more heat into a larger amount of mechanical work to produce more electricity.
- Supercritical reservoirs at high temperature and pressure, beyond the critical point, could provide more than 20 times as much enthalpy per cubic meter as the geothermal fluids used with present current technology.
- Deep geothermal heat will be able to generate, in the next future, more electricity, more efficiently, cleaner energy, through special advanced turbine-generators adapted for supercritical fluids.

7. APPENDIX

The mathematical formulation **IAPWS-95** for the calculation of the thermodynamic properties of geothermal water was built by the *International Association for the Properties of Water and Steam* (<http://www.iapws.org>). This Appendix extends this formulation to include the calculation of isothermal compressibility and thermal expansivity, improving the important option of calculating water properties as functions of fluid pressure and temperature. The IAPWS-95 takes temperature T (K) and density ρ [kg/m³] as arguments of its equations. This section contains efficient and accurate algorithms for the backward inversion of internal correlations in this formulation, making all properties functions of pressure (bar) and temperature (°C) in single-subcritical phase, liquid or steam, and for the supercritical phase. For two-phase water p_{sat} and T_{sat} are not independent, but related in the saturation line through the so-called Function- K . The IAPWS-95 calculates p_{sat} as function of temperature. This extended formulation, contains a very accurate inversion algorithm, which computes T_{sat} as function of the saturation pressure p_{sat} . To calculate all the variables of the two-phase fluid, another variable is required, for example steam quality, liquid saturation or fluid enthalpy, which is also included herein. The original document was published recently (Suárez-Arriaga, 2017a) as the first full Spanish expanded version of the IAPWS-95 formulation. It includes the development of a computational code that complements this formulation (Suárez-Arriaga, 2017b), which is available to the interested public.

The main function used in the IAPWS-95 is the reduced Helmholtz potential Φ , which is composed of two parts, the ideal gas part Φ^0 , and the residual part Φ^r . The main thermodynamic reduced variables are the reduced temperature θ , the reduced density δ , and the reduced inverse of temperature $\tau = \theta^{-1}$. These variables are defined in equation (2). The mathematical form of the ideal gas part (Φ^0) and the residual part (Φ^r) of Φ are respectively:

$$\begin{aligned}\Phi_{gas}^{ideal} &= \Phi^0(\delta, \tau) = \text{Log}(\delta) + n_{01} + n_{02} \tau + n_{03} \text{Log}(\tau) + \sum_{i=4}^8 n_{0i} \text{Log}(1 - e^{-\gamma_{0i} \tau}) \\ \Phi^r(\delta, \tau) &= \sum_{i=1}^7 n_i \delta^{d_i} \tau^{t_i} + \sum_{i=8}^{51} n_i \delta^{d_i} \tau^{t_i} e^{-\delta^{\epsilon_i}} + \sum_{i=52}^{54} n_i \delta^{d_i} \tau^{t_i} e^{-\alpha_i(\delta - \epsilon_i)^2 - \beta_i(\tau - \gamma_i)^2} + \sum_{i=55}^{56} n_i \Delta^{b_i} \delta \psi\end{aligned}\quad (13)$$

where the auxiliary functions are defined as follows:

$$\Delta(\delta) = \Theta^2 + B_i (\delta - 1)^{2a_i}; \quad \Theta(\delta, \tau) = 1 - \tau + A_i (\delta - 1) \frac{1}{\beta_i}; \quad \psi(\delta, \tau) = e^{-C_i(\delta - 1)^2 - D_i(\tau - 1)^2}\quad (14)$$

All numerical coefficients included in these formulae, are defined and detailed in the official reference (IAPWS R6-95, 2016). The combination of both parts of the dimensionless potential Φ define a full Helmholtz surface given by equation (2). Other thermodynamic properties of water are obtained by partial differentiation over the Helmholtz potential or free energy surface:

$$\begin{aligned}p &= \rho^2 \left(\frac{\partial f_w}{\partial \rho} \right)_T, \quad e = f_w - T \left(\frac{\partial f_w}{\partial T} \right)_\rho, \quad h = f_w - T \left(\frac{\partial f_w}{\partial T} \right)_\rho + \rho \left(\frac{\partial f_w}{\partial \rho} \right)_T, \quad s = - \left(\frac{\partial f_w}{\partial T} \right)_\rho \\ c_V &= \left(\frac{\partial e}{\partial T} \right)_V, \quad c_p = \left(\frac{\partial h}{\partial T} \right)_p, \quad C_f = \frac{1}{\rho} \left(\frac{\partial \rho}{\partial p} \right)_T, \quad J = \left(\frac{\partial T}{\partial p} \right)_h, \quad v_s = \sqrt{\left(\frac{\partial p}{\partial \rho} \right)_s}, \quad \gamma_f = \frac{-1}{\rho} \left(\frac{\partial \rho}{\partial T} \right)_p\end{aligned}\quad (15)$$

where symbols h , s , c_V , c_p , C_f , J , v_s and γ_f are specific enthalpy, specific entropy, isochoric and isobaric heat, isothermal compressibility, Joule-Thomson coefficient, sound speed and isobaric thermal expansion respectively. Thermal diffusivity can also be computed as follows: $\delta_f = k_T / \rho c_p$, where k_T is the thermal conductivity of the fluid. All the properties given in equation (15) are computed in terms of the dimensionless parts of the Helmholtz potential:

$$\begin{aligned}
16a). \quad p(\delta, \tau) &= R \rho_C T_C \tau^{-1} \left(\delta + \delta^2 \frac{\partial \Phi^r}{\partial \delta} \right), \quad 16b). \quad e(\delta, \tau) = R T \tau \left(\frac{\partial \Phi^0}{\partial \tau} + \frac{\partial \Phi^r}{\partial \tau} \right), \\
16c). \quad h(\delta, \tau) &= R T \left(1 + \tau \left(\frac{\partial \Phi^0}{\partial \tau} + \frac{\partial \Phi^r}{\partial \tau} \right) \right), \quad 16d). \quad s(\delta, \tau) = R \left(\tau \left(\frac{\partial \Phi^0}{\partial \tau} + \frac{\partial \Phi^r}{\partial \tau} \right) - \Phi^0 - \Phi^r \right), \\
16e). \quad c_V(\delta, \tau) &= -R \tau^2 \left(\frac{\partial^2 \Phi^0}{\partial \tau^2} + \frac{\partial^2 \Phi^r}{\partial \tau^2} \right), \quad 16f). \quad c_p(\delta, \tau) = R \left(-\tau^2 \left(\frac{\partial^2 \Phi^0}{\partial \tau^2} + \frac{\partial^2 \Phi^r}{\partial \tau^2} \right) + \frac{1 + \delta \frac{\partial \Phi^r}{\partial \delta} - \delta \tau \frac{\partial^2 \Phi^r}{\partial \delta \partial \tau}}{1 + 2 \delta \frac{\partial \Phi^r}{\partial \delta} + \delta^2 \frac{\partial^2 \Phi^r}{\partial \delta^2}} \right) \\
16g). \quad K_f(\delta, \tau) &= \frac{R \rho_C T_C}{\tau} \left(\delta + 2 \delta^2 \frac{\partial \Phi^r}{\partial \delta} + \delta^3 \frac{\partial^2 \Phi^r}{\partial \delta^2} \right), \quad 16h). \quad C_f(\delta, \tau) = \frac{1}{K_f(\delta, \tau)} \\
16i). \quad v_S(\delta, \tau) &= \sqrt{R T \times 10^3 \left(1 + 2 \delta \frac{\partial \Phi^r}{\partial \delta} + \delta^2 \frac{\partial^2 \Phi^r}{\partial \delta^2} - \frac{\left(1 + \delta \frac{\partial \Phi^r}{\partial \delta} - \delta \tau \frac{\partial^2 \Phi^r}{\partial \delta \partial \tau} \right)^2}{\tau^2 \left(\frac{\partial^2 \Phi^0}{\partial \tau^2} + \frac{\partial^2 \Phi^r}{\partial \tau^2} \right)} \right)} \\
16j). \quad \gamma_f(\delta, \tau) &= \frac{\tau^2}{T_C \delta} \left(\frac{\partial \delta}{\partial \tau} \right)_{\Pi}, \quad 16k). \quad \delta_f(\delta, \tau) = \frac{k_T}{\rho_C \delta c_p(\delta, \tau)}
\end{aligned} \tag{16}$$

where $\partial \Phi / \partial \delta$, $\partial \Phi / \partial \tau$ and $\partial \Phi / \partial \delta \partial \tau$ are the partial derivatives with respect to the dimensionless variables (δ, τ) of the reduced Helmholtz potential. Thermal conductivity of water, including a critical enhancement, is calculated separately (IAPWS-95, 2011):

$$\begin{aligned}
\theta &= \frac{T}{T_C} = \tau^{-1}, \quad \lambda_2(\delta, \tau) = \frac{\Lambda}{\tau} \frac{\delta c_p(\delta, \tau) \mu_c}{R \mu_{f0}} Z(y_0) \Rightarrow k_T(\theta, \delta) = \lambda_0(\theta) \lambda_1(\theta, \delta) + \lambda_2(\theta, \delta) \\
\lambda_0(\tau) &= \sqrt{\tau^{-1}} \left(\sum_{i=0}^4 L_i \tau^i \right)^{-1}; \quad \lambda_1(\delta, \tau) = \text{Exp} \left[\delta \sum_{i=0}^4 (\tau-1)^i \times \sum_{j=0}^5 L(i, j) (\delta-1)^j \right]
\end{aligned} \tag{17}$$

Dynamic viscosity is computed as follows (IAPWS R6-95, 2016):

$$\mu_w(\delta, \theta) = \mu_0(\delta, \theta) \mu_1(\delta, \theta), \quad \theta = \tau^{-1}, \quad \mu_0 = 100 \sqrt{\theta} \left(\sum_{i=0}^3 \frac{H_i}{\theta^i} \right)^{-1}, \quad \mu_1 = \text{Exp} \left[\delta \sum_{i=0}^5 \left(\frac{1}{\theta} - 1 \right)^i \sum_{j=0}^6 H_{ij} (\delta-1)^j \right] \tag{18}$$

7.1 Brief discussion of the limits for IAPWS-95 formulation

This formulation is presented here succinctly and is valid throughout all the water stable region, from 273.16 K (0.01°C) to 1273 K (1000°C) and for any positive pressure $p > 0$ up to 1000 MPa (10,000 bar). By extrapolation, the applicability of equations (16b, 16c and 16d) for enthalpy, internal energy and entropy at the supercritical limit of 4727°C and 10^6 bar can be reasonably extended. The absolute limits, after which calculations can no longer be made, are $T = 190$ K (-83°C) and $T > 5000$ K (4727°C), for $p > 10^5$ MPa (10^6 bar). In terms of practical applications, the formulation represented by equations (16) [2, 12] can certainly be used in the geothermal ranges $T \in [0^\circ\text{C}, 1000^\circ\text{C}]$ and pressures $p \in [0.01, 1000]$ bar, which include magmatic conditions. The full description of the derivatives of functions in equations (16) and of all numerical coefficients are found on the webpage (<http://www.iapws.org/>).

7.2 Computation of the isothermal compressibility using the IAPWS-95 formulation

The same reduced Helmholtz potential can be used to build the precise formula for isothermal compressibility (equation 16h). Let Π be the dimensionless reduced pressure $\Pi = p/P_C$, then from the definition of fluid compressibility and using equation (16a):

$$\begin{aligned}
C_f &= -\frac{1}{v_f} \left(\frac{\partial v_f}{\partial p} \right)_T = \frac{1}{\rho_f} \left(\frac{\partial \rho_f}{\partial p} \right)_T, \quad p = \rho^2 \left(\frac{\partial f_w}{\partial \rho} \right)_T = \rho^2 R T \left(\frac{1}{R T} \frac{\partial f_w}{\partial \rho} \right)_T = \rho^2 R T \frac{\partial \Phi}{\partial \rho} \\
\Rightarrow \frac{p(\delta, \tau)}{R \rho T} &= \rho \frac{\partial \Phi}{\partial \rho} = \frac{\rho_C \delta}{\rho_C} \frac{\partial \Phi}{\partial \delta} = \delta \left(\frac{\partial \Phi^0}{\partial \delta} + \frac{\partial \Phi^r}{\partial \delta} \right) = 1 + \delta \frac{\partial \Phi^r}{\partial \delta}
\end{aligned} \tag{19}$$

Developing this expression using fluid compressibility definition within the same equation (19):

$$C_f = \frac{1}{\rho} \left(\frac{\partial \rho}{\partial p} \right)_T = \frac{\chi_C}{\rho_C \delta} \frac{\partial \delta}{\partial p} = \frac{1}{P_C \delta} \frac{\partial \delta}{\partial \Pi} \Rightarrow \frac{1}{C_f} = K_f(\delta, \tau) = P_C \delta \frac{\partial \Pi}{\partial \delta}; \quad \Pi = \frac{p}{P_C} \quad (20)$$

$$\Rightarrow \boxed{\frac{1}{C_f(\delta, \tau)} = K_f(\delta, \tau) = R \rho_C T \delta^2 \left(\frac{1}{\delta} + 2 \frac{\partial \Phi^r}{\partial \delta} + \delta \frac{\partial^2 \Phi^r}{\partial \delta^2} \right)}$$

where K_f is the bulk modulus of water and the inverse function of compressibility. It is important to notice that equation (21) is fully compatible with IAPWS-95, because it uses same derivatives and functions. Another important derivative can be deduced from previous equations (20):

$$\frac{\partial \Pi}{\partial \delta} = \frac{K_f(\delta, \tau)}{P_C \delta} = \frac{R \rho_C T}{P_C} \left(1 + 2\delta \frac{\partial \Phi^r}{\partial \delta} + \delta^2 \frac{\partial^2 \Phi^r}{\partial \delta^2} \right) \Rightarrow \boxed{C_f(\delta, \tau) = \frac{1}{P_C \delta} \frac{\partial \delta}{\partial \Pi}} \quad (21)$$

Equation (21) is the equivalent form, using dimensionless variables, of isothermal fluid compressibility, which is equal to the partial derivative of reduced density with respect to reduced pressure, divided by reduced density and by P_C .

7.3 Computation of thermal expansivity using the IAPWS-95 formulation

Using the definition of thermal expansivity under constant pressure and dimensionless variables:

$$\gamma_f = \frac{-1}{\rho} \left(\frac{\partial \rho}{\partial T} \right)_p = \frac{-1}{\rho_C \delta} \frac{\partial (\rho_C \delta)}{\partial (T_C \tau^{-1})_p} = \frac{\tau^2}{T_C \delta} \left(\frac{\partial \delta}{\partial \tau} \right)_p \quad (22)$$

Using again equation (16a) in dimensionless form and combining with equation (22), and after some algebra:

$$p(\delta, \tau) = R \rho_C T_C \frac{\delta}{\tau} \left(1 + \delta \frac{\partial \Phi^r}{\partial \delta} \right) = cte \Leftrightarrow \frac{\partial p}{\partial \delta} = \frac{\partial p}{\partial \tau} = 0 \Rightarrow$$

$$\boxed{\gamma_f(\delta, \tau) = \frac{R \rho_C}{P_C} \left(1 + \delta \frac{\partial \Phi^r}{\partial \delta} - \tau \delta \frac{\partial^2 \Phi^r}{\partial \tau \partial \delta} \right) \frac{\partial \delta}{\partial \Pi} = R \rho_C \delta C_f \left(1 + \delta \frac{\partial \Phi^r}{\partial \delta} - \tau \delta \frac{\partial^2 \Phi^r}{\partial \tau \partial \delta} \right)} \quad (23)$$

REFERENCES

- Bundschuh, J., and Suárez-Arriaga, M.C.: *Introduction to the Numerical Modeling of Groundwater and Geothermal Systems – Fundamentals of mass, energy and solute transport in poroelastic rocks*. (London UK, Leiden, The Netherlands; 1st Edition, Multiphysics Modeling Series 2, CRC Press/Balkema – Taylor & Francis Group, (2010), 1-479 <Reference Style>
- de la Calleja, E.: Unpublished internal report. Instituto de Investigación en Materiales – UNAM, (2018).
- DiPippo R, 2008. *Geothermal Power Plants - Principles, Applications, Case-Studies and Environmental Impact*, Chapter 10: *Exergy Analysis Applied to Geothermal Power Systems*. Ed. Butterworth-Heinemann.
- Harvey, A.H., Peskin, A.P. and Klein, S.A.: NIST/ASME Steam Properties: Users' Guide, version 2.21, *NIST Standard Reference Database 10*, National Institute of Standards and Technology, U.S. Department of Commerce, (2004).
- IAPWS-95: *Release on the IAPWS Formulation 2011 for the Thermal Conductivity of Ordinary Water Substance* (Plzeň, Czech Republic: International Association for the Properties of Water and Steam, (2011), 1-15.
- IAPWS R6-95: *Formulation 1995 for the Thermodynamic Properties of Ordinary Water Substance for General and Scientific Use* The Netherlands 2009; Revised Release Dresden, Germany 2016: International Association for the Properties of Water and Steam, (2016), 1-18.
- Suárez-Arriaga, M.C., Bundschuh, J. and Samaniego, F.: Assessment of submarine geothermal resources and development of tools to quantify their energy potentials for environmentally sustainable development. *J. of Cleaner Production* **83**, (2014), 21-32.
- Suárez-Arriaga, M.C.: Propiedades termodinámicas del agua geotérmica con la formulación IAPWS-95 programada y ampliada. *GEOTERMIA-Rev. Mex. de Geoenergía* **30/2**, (2017a), 6-19.
- Suárez-Arriaga, M.C.: The Equation of State for Water IAPWS-95 programmed in Mathematica 11.2. *Wolfram Technical Conference*, Champaign, Ill. (2017b), 1-13.